DYNAMICS OF BLUE-VIOLET InGaN LASERS WITH DIFFERENT SATURABLE ABSORBER DESIGNS

V.Z. Tronciu

Department of Physics, Technical University of Moldova, 168 bd. Stefan cel Mare, MD-2005, Chisinau, Republic of Moldova
E-mail: tronciu@mail.utm.md

Abstract

A review is presented of a range of investigations of the CW, self-pulsating and excitable behaviour of blue-violet InGaN lasers with different designs of saturable absorber. Bifurcations have been identified that are the origin of the phenomena and different device designs are considered that are intended to control the laser behaviour in BD applications. It is found that the properties of the saturable absorber strongly affect the self-pulsation and excitability properties of the lasers. The influence on laser dynamics of other device and material parameters has also been investigated. Very encouraging agreement between the results of numerical calculations and the experimental data on self-pulsating laser operation is demonstrated.

1. Introduction

During the recent years, violet InGaN lasers have received considerable attention for applications in high-density optical disk storage and optical data processing. In particular, laser diodes operating at a wavelength around 400nm are required for Blu-ray Disc (BD) systems if disk storage capacity is to be increased up to 25 Gbytes (see Figure 1). BD is the name of a next-generation optical disc format. The format offers more than five times the storage capacity of traditional DVDs [1]. Much progress in the developments of violet-blue lasers has been made since the first operation of such a laser was reported by Nakamura et. al. [2, 3]. Meanwhile, several groups have reported continuous-wave (CW) operation at room temperature using different fabrications methods [4-8]. Recently, violet laser diode performance has been improved and the lifetime has been extended to over 15000h and 400nm CW laser diodes (LDs) are already available commercially [9]. However, since the early investigation by Nakamura [10], self-pulsating violet LDs have neither been reported nor studied in detail.

A laser is considered to produce self-pulsation (SP) if the output is a periodic train of pulses for a constant injected current. The phenomenon of SP in semiconductor lasers, has been found to be effective in reducing mode hopping noise and also optical feedback noise in optical disk systems (compact disk and video disk players etc.) [11-13]. Also the modal noise in multimode fibre links and communication systems (multimode fibre communication networks, and optical interconnects) is reduced by self-pulsating operation. Recently, self-pulsating lasers have been used for optical clock recovery, which is a key functionality required for optical signal processing [14-16]. Self-pulsating operation is achieved mainly with two types of lasers; lasers with a saturable absorber (absorptive Q-switching) [17,18] and the more recent multi-section DFB lasers (with dispersive Q-switching and mode beating) [19, 20]. In the latter case, very high frequencies can be achieved (up to 100GHz) and the frequency can be tuned electrically and continuously over a wide range [21].

Excitability and coherence resonance are rapidly expanding topics in optics, having been initially studied in biology [22] and chemistry [23]. Recently the phenomenon of excitability has been predicted to occur in optical devices such as cavities [24, 25], different types of lasers [26-28] etc. and convincing experimental evidence of excitability in a laser with a short external cavity is reported in [29]. In addition, an experimental investigation of the excitable properties of a solid-state laser with an intra-cavity saturable absorber (SA) is reported by Larotonda et al [30].

In this review, we focus on an investigation of the phenomena of SP, excitability and coherence resonance of blue-violet InGaN lasers with different SAs. These investigations extend and complement previous studies of blue laser dynamics [31-36]. It is shown how different laser structures can be used to control device behaviour and the dependence of SP and excitability on laser geometry. The structure of the paper is as follows. In Section 2, we present the laser structure, the physical model and the equations for the case of the SA layer grown parallel to the active region. Numerically simulated results and experimental data of a self-pulsating InGaN laser are presented and good agreement between the measured and calculated characteristics of InGaN lasers SP is demonstrated. Also in Section 2, we study how the laser and material parameters influence the laser dynamics and show that excitability can occur. Section 3 is devoted to a presentation of laser designs and a model of a tandem blue laser. The simulation results and discussions presented are based on single mode rate equations. Finally, conclusions are given in Section 4.

2. Blue lasers with saturable absorber

2.1. Model and equations

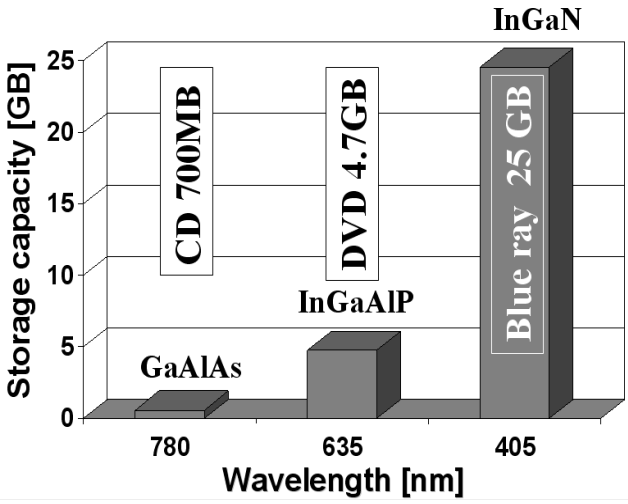

Figure 1. The dependence of storage capacity of disks on the laser wavelength.

Figure 2 is a schematic diagram of the type self-pulsating laser structure considered, which is based on lasers that have been fabricated in practice [37, 31]. The device consists of an InGaN active layer and a p-type InGaN layer acting as a saturable absorber. The active layer is composed of 6 quantum wells (wells of $In_{0.07}Ga_{0.93}N$; barriers of $In_{0.02}Ga_{0:98}N$), while the saturable absorber consists of a single quantum well. The thickness of the saturable absorber is set in the range 1nm to 3nm. Most of numerical calculations reported in this paper have been carried out for lasers with a SA of 3nm thickness because a thin layer is preferable to prevent a large threshold current. On the other hand, an excessively thin SA layer substan-

tially reduces the operating range of the SP. The p-type AlGaN layer is intended to suppress carrier evaporation between the active region and the SA [37].

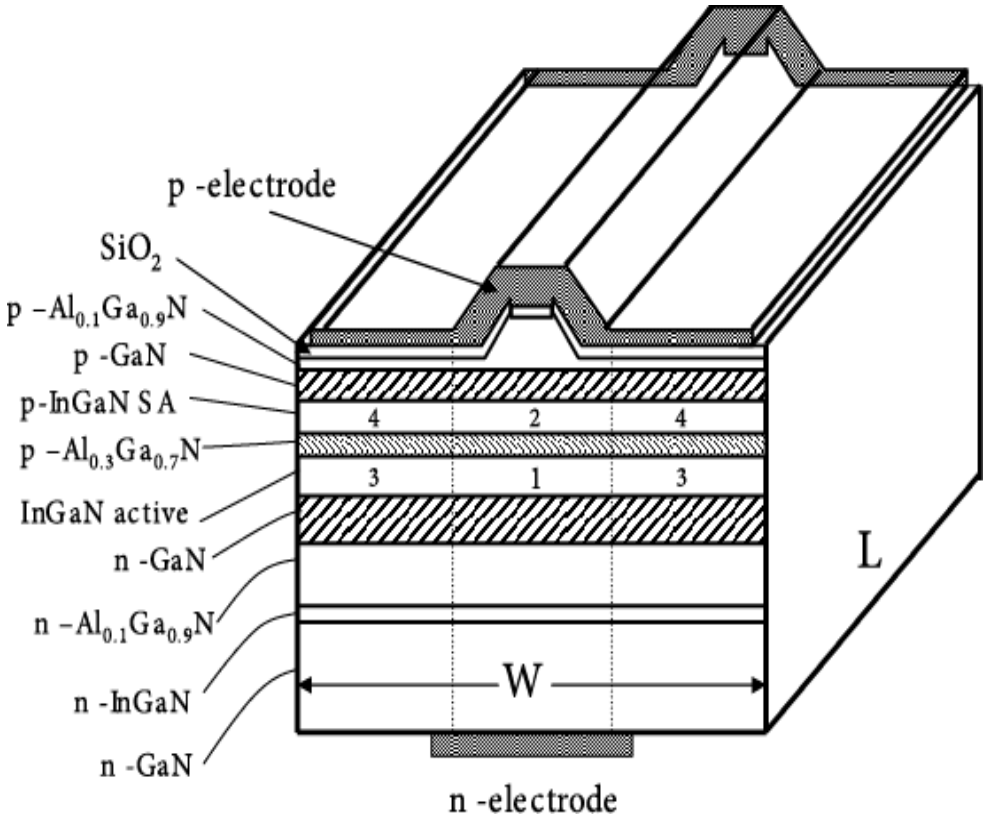

Figure 2. Schematic illustration of a blue-violet InGaN laser with a saturable absorber [37,32].

The model used in this paper was first proposed by Yamada [38, 39]. The equations of laser operation are

$$\frac{dS}{dt} = \left[\sum_i a_i \xi_i (N_i - N_{gi}) / V_i - BS - G_{th} \right] S + M \sum_i a_i \xi_i N_i / V_i \qquad (1)$$

$$\frac{dN_i}{dt} = -\frac{a_i \xi_i}{V_i} (N_i - N_{gi}) S_i - \frac{N_i}{\tau_{si}} + \sum_{j \neq i} \left(\frac{N_j}{T_{ji}} - \frac{N_i}{T_{ij}} + \frac{(I_{ji} - I_{ij})}{e} \right) \qquad (2)$$

where i and j label the layers of the central and outer regions, respectively (see Figure 2). S is the photon number, N_i is the injected carrier number in the central region i, and N_j is the same in the outer region j. a_i is the differential gain coefficient, ξ_i is the field confinement ratio, N_{gi} is the transparent carrier number, τ_{si} is the carrier lifetime, and T_{ij} is an equivalent lifetime giving the carrier diffusion from region i to j. I_{ji} gives the carrier injection from region j to i, M is the equivalent total number of longitudinal modes $M = \Delta\omega n_r L / 2c$ [40] and V_i is the volume expressed by $V_i = W_i d_i L$, where L is the laser length, and d_i and W_i are respectively the thickness and width of region i. B is the gain saturation coefficient $B = B_c(N - N_{g1})$ where

$$B_c = \frac{9\pi c \tau_{in}^2}{2\varepsilon_0 n_r^2 \hbar \lambda_0} \frac{\left| R_{cv} \right|^2 a_1 \xi_1^2}{V_1^2} \qquad (3)$$

in which n_r is the refractive index, which is calculated by the first-order Sellmeier equation $n_r = \sqrt{b_1 + \lambda^2/(\lambda^2 - b_2)}$, where b_1 and b_2 are the fitting parameters (b_1=4.37 and b_2=8.76×10^{4}m^2). λ_0 is the central wavelength of the laser, R_{cv} is the dipole moment, and τ_{in} is the intra-band relaxation time. The other parameters correspond to the active region ($i = 1$). The threshold gain level G_{th} is given by

$$G_{th} = \frac{c}{n_r}\left(k + \frac{1}{2L}\ln\frac{1}{R_f R_B}\right) \tag{4}$$

where R_f and R_b are the reflectivity at the front and the back facets, respectively. k is the loss coefficient. Parameters used in the calculations of Figures 3-10 are as shown in Table 1.

Table 1. Parameters used in numerical calculations

Symbol	Definition	Value & units	
		Active region	SA
a	Differential gain coefficient	1.85 ×10^{-12} m^{3}s^{-1}	13.0 ×10^{-12}m^{3}s^{-1}
N_g	Transparent carrier density	1.4×10^{25}m^{-3}	2.6×10^{25}m^{-3}
τ_s	Carrier lifetime	1.8-2.0 ns	0.1 ns
d	Thickness	18nm	3 nm
W	Width	2.0μm	2.0μm

Other parameters

k	Loss coefficient	15cm^{-1}
I_l	Leak current	0.35I
R_b	Reflectivity at back facet	0.95
R_f	Reflectivity at front facet	0.20

2.2 CW and self-pulsating operations

As mentioned in section 1, SP can play an important role when semiconductor lasers are used to read optical-storage disks because self-pulsating lasers are less sensitive to optical feedback. As a result, the use of SA to produce self-pulsating operation has been investigated for many years in stripe-geometry lasers [41-43] and in double-section laser diodes [44]. Recently, dispersive switching mechanism has been used to describe SP in multi-section distributed feedback (DFB) lasers [45-47]. A lot of effort has been devoted to explaining the phenomenon and several models have been developed, which predict SP as well as other kinds of behavior, such as bistability, excitability and chaos. However, in general, the physical mechanism of SP for lasers with a saturable absorber is the following [38]. In the absence of photons in the active region, the electron density there is increased by injected current; when the electron density approaches threshold, photons start to be generated and are absorbed in the absorber; hence the electron density in the absorber is increased, the photon absorption rate is reduced and the photon density is increased further; the electron density in the active region is then reduced as a result of stimulated emission and laser operation ceases. The process then repeats itself, which in semiconductor lasers produces pulses with a typical frequency of the order of several gigahertz.

In particular, it has been shown [37, 31] that in the case of a laser with a 650 μm cavity length, SP can be achieved experimentally for an injected current in the range from 163 to 220

mA with a frequency range of 1.6 to 2.25 GHz. A typical experimental oscilloscope trace is shown in Figure 3(a) for SP, which was almost stable during the 1.6 μs pulse duration of the injection current. Figure 3(b) shows the calculated pulse trace for the same laser with an injected current of 185 mA. The frequency of the pulsation shown in Figure 3(b) coincides with that of Figure 3(a) and is approximately 2 GHz.

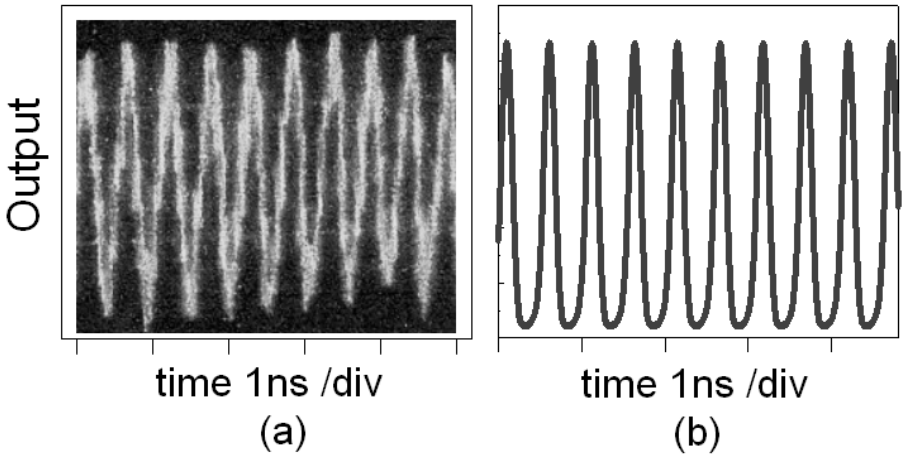

Figure 3. (a) Measured [37], and (b) calculated [31] pulse traces of a 650-μm cavity length laser with 185-mA injected current. The other parameters are as in Table I.

The predicted region of self-pulsation is shown in the plot of laser cavity length versus injected current shown in Figure 4. The solid line indicates the position of a Hopf bifurcation, which gives the boundary between CW and self-pulsating operation. This line has been calculated using equations (1)–(5) with InGaN laser parameters (see Table 1). The dashed line shows the threshold current. The experimentally determined ranges of the self-pulsation for different cavity lengths are indicated with dotted lines terminated by block squares. In the case of the laser with a 650μm cavity length, the upper limit of 220mA is actually that of the current generator used, rather of the SP. It is clear from the figure that experiment and theory generally agree very well. The main conclusions are that the foolowing: 1) The self-pulsation region increases with cavity length; 2) A shorter laser cavity length gives a lower threshold current and eventually leads to the disappearance of the SP region; 3) The cavity length range from 350 to 650μm can be considered to be suitable for SP in the InGaN lasers.

We next examine the laser dynamics in terms of bifurcation diagrams. A typical calculation of bifurcation for the periodic solution is shown in Figure 5, which shows the dependence of peak photon number on injected current. When the injected current is increased, CW operation is observed (thin solid line) from just above the threshold current but pulsations begin when the Hopf bifurcation (marked by a circle) is reached. This behaviour differs from that of other self-pulsating lasers reported in [38, 48, 49], where the self-pulsation starts at the threshold current. In the previous work, the carrier lifetime in the SA region is assumed to be the same as that in the active region. However, the carrier lifetime of the SA region in this paper is set to be 0.1 ns, which is much smaller than 2.0 ns in the active region but is in line with experimental observation and is believed to be caused by piezoelectric and tunnelling effects, in the single-quantum-well structure [37, 50, 51]. After the Hopf bifurcation the pulsation amplitude reaches a maximum and then declines eventually disappearing at the upper Hopf point. Both Hopf points are supercritical.

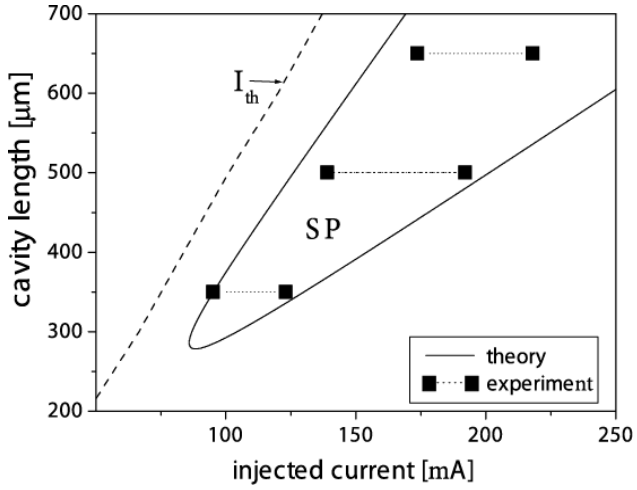

Figure 4. Self-pulsation region in the plane of the laser cavity length vs injected current. The dashed line indicates the threshold current. Experimentally measured ranges [37] of the self-pulsation are indicated with dotted lines terminated by block squares.

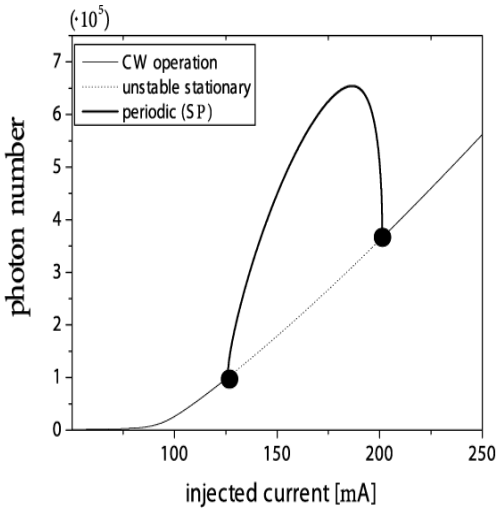

Figure 5. A bifurcation diagram for a laser with a 500μm cavity length. The other parameters are as in Table 1.

In order to estimate the SP frequency, numerical simulations were carried out in the parameter plane of cavity length versus injected current. The results are shown in Figure 6, where the darker regions correspond to SP and the white region to CW operation or no lasing. It can be clearly seen how the SP frequency changes in the plane of the two parameters and, in particular, how for a fixed injected current the pulsation frequency becomes higher as the cavity length is reduced.

In addition, we can consider the influence of other device and material parameters on the laser dynamics. Figure 6 (b) shows the frequencies calculated for the SP region in the parameter plane of SA and active region differential gain coefficients. The laser cavity length is 500μm, the injected current is fixed at 100mA and the other parameters fixed as in Table 1.

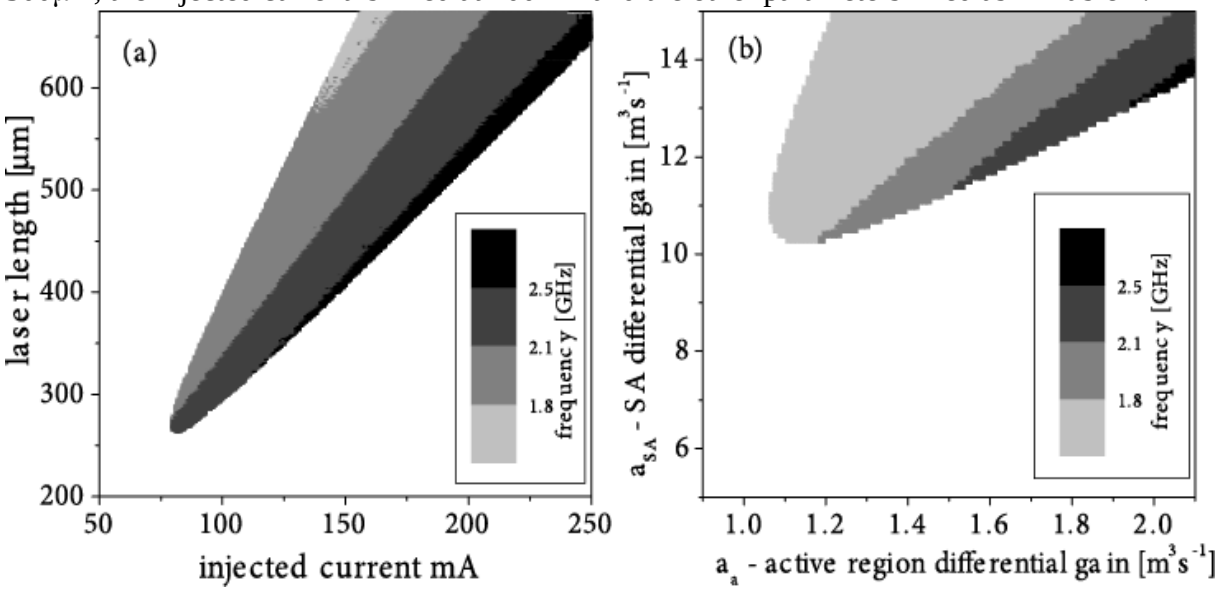

Figure 6. Calculated variation of the SP frequency in the plane of different parameters: a) the cavity length vs injected current, b) SA vs active region differential gain. For case b) the injected current is fixed to 100 mA. The other parameters are as in Table 1.

First we consider the possible variation of differential gain in the active region and in the SA. Note that the white background again corresponds to non-lasing or CW operations.

For $a_{active}<1.0\times10^{-12}m^3s^{-1}$ the laser shows CW, but not SP, operation. For $a_{active} > 1.0\times10^{-12}m^3s^{-1}$ SP is possible but exceeding a critical level of differential gain in the active region is not a sufficient condition to get SP since its existence also depends on the level of differential gain in the SA. It is apparent from Figure 6(b) that the SP frequency increases with the differential gain coefficient in the active region but a corresponding increase in the differential gain in the SA is necessary if SP is to occur.

Next, we investigate the influence of different parameters on the SP. It has been estimated [2, 3] that the carrier lifetime in an InGaN multi-quantum well laser diode is typically between 1.8ns and 3ns. In our calculations we have used 2ns in the active region but the same value is considered to be very large for the SA. It is also worth noting that SP has been seen [37] in an InGaN laser with a very short SA carrier lifetime but not in devices with large SA carrier lifetime. With regard to measurements relevant to SAs, it has recently been found that the quantum well carrier lifetime drastically decreases from 2.5ns to 2ps with increasing reverse bias [50]. This decrease has been attributed to carrier escape by tunneling through tilted barriers. Also, a room temperature study of the dependence of carrier lifetime on well width in an InGaN single quantum well [51] found the carrier recombination to be dominated by nonradiative processes. Within the quantum well thickness range from 1nm to 6 nm, the carrier lifetime was found to increase from 180ps to 340ps. In this paper a SA carrier lifetime of 0.1 ns has been used unless otherwise stated. However, in Figure 7(a) we examine the effect on SP of varying the carrier lifetimes in the active region and the SA for two values of SA thickness d_{SA}, while keeping all other parameters with the values given in Table 1.

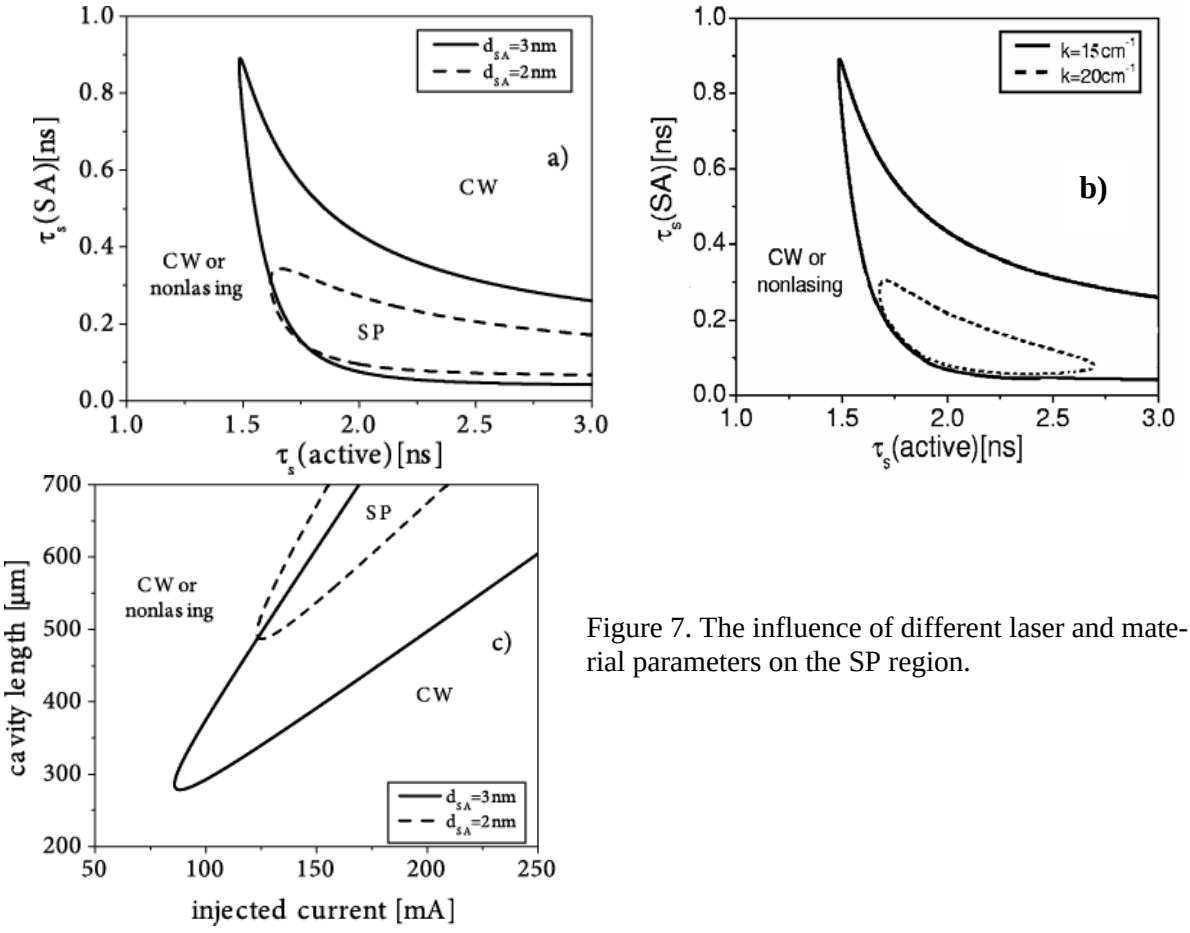

Figure 7. The influence of different laser and material parameters on the SP region.

The results predict that when the carrier lifetime in the active region is smaller than 1.5ns, only CW operation occurs and that a large τ_s in the active region requires a relatively low value of the carrier lifetime in the SA for SP operation to occur. In Figure 7b we show the corresponding diagram (with d_{SA} = 3nm) for two different values of the optical loss coefficient: $k = 15cm^{-1}$ (solid line) and $k = 20cm^{-1}$ (dashed line). It can be seen that an increase in the loss coefficient results in a substantial shrinkage of the SP region.

Now we consider the influence of the SA thickness d_{SA} on the laser properties. The thickness of the SA affects the field confinement factor, the carrier lifetime, and the carrier overflow. Figure 7c shows the SP region in the parameter plane of cavity length versus the injected current for different values of thickness of the SA. The lines in Figure 7c represent the boundaries between the CW and SP regions. The variation of the thickness from 1 to 3 nm is considered to be appropriate for our fabricated lasers. For the thinner SA, the SP region becomes much smaller. This behaviour can be explained by recognizing that the decrease of the SA thickness results in a smaller optical confinement factor. A reduction of SA thickness also leads to a lower threshold current. Thus, we conclude that thinner SAs imply lower threshold currents but reduced SP regions.

2.3 Excitability

Excitability in optics is potentially of great interest because of the prospects for applications in optoelectronic devices, primarily for optical switching, clock recovery, pulse reshaping and the generation of a coherence resonance output of pulses. General bifurcation analysis related to excitability in different types of laser is reported in [27] but here we discuss specifically the mechanism of excitability for a blue InGaN laser suitable for practical applications. We begin by considering what is predicted to happen if the carrier lifetime in the SA is increased from 0.1 ns to 2 ns for a laser with a cavity length of 650 μm and a SA thickness of 2 nm. The results of the numerical calculations of photon number against injected current are shown in Figure 8.

For a SA with a carrier lifetime of 0.1 ns, the laser exhibits SP as a result of the Hopf bifurcations marked by the squares in Figure 8a. With increasing SA carrier lifetime, the pulsation region decreases as shown in Figure 8b. The carrier lifetime of 1.4 ns, to which Figure 8c refers, is considered the critical value, after which the hysteresis phenomenon implicit in Figure 8d (corresponding to a lifetime of 2 ns) appears. A further increase of SA carrier lifetime is accompanied by a decrease of the size of the pulsation region and more pronounced hysteresis. A linear stability analysis shows that the lower branch of the hysteresis curve is stable while the upper one is unstable. For the same current, a stable node, a saddle, and an unstable focus are present, providing conditions that can result in excitable behaviour. In fact, we have found that when the operating point is situated in the current range denoted by (e) in Figure 8d, the laser is excitable. We have also found that the phenomenon of excitability becomes more pronounced as the cavity length is increased. We note that excitability has been predicted to occur when the carrier lifetimes in the active and SA regions are the same, in contrast to the conditions for SP, where a significantly shorter lifetime in the SA is required. This means that excitability could be achieved in practice in a device, where the saturable absorber is made of the same material as the active region and is located next to it in the longitudinal direction. An alternative approach to obtaining excitability is to have a suitable value for the absorption level. Figure 9 shows a bifurcation diagram in the plane of SA differential gain coefficient versus injected current for a laser with a cavity length of 650 μm and carrier lifetimes of 2 ns and 0.5 ns in the active and SA regions, respectively.

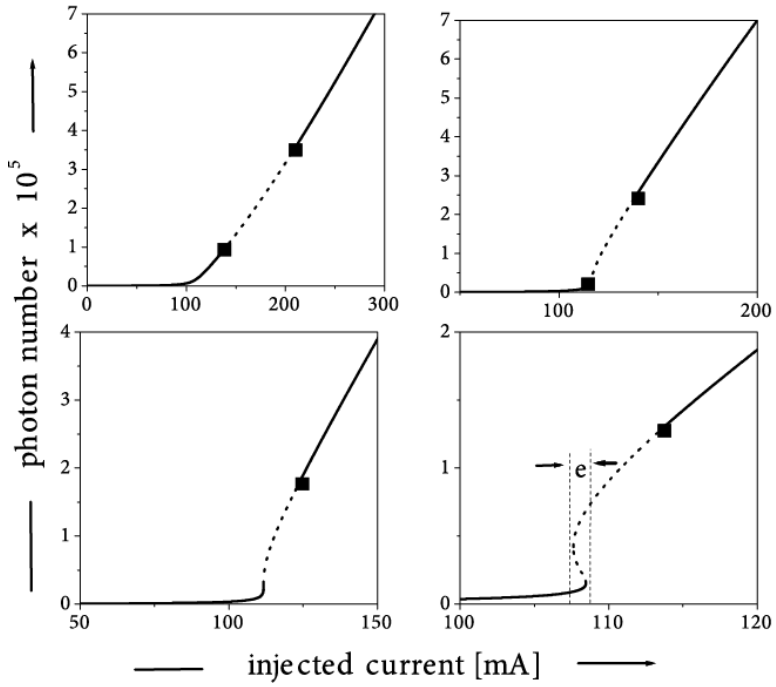

Figure 8. Dependence of stationary photon number S on the injected current for different values of the carrier lifetime in the saturable absorber. The cavity length is 650 μm and the carrier lifetime is *a*) $\tau_S(SA) = 0.1ns$, *b)* τ_s(SA) = 1.0 ns, c) τ_s(SA) = 1.4 ns, *d)* τ_s(SA) = 2.0 ns. The thickness of the saturable absorber is 2 nm. The other parameters are as in Table 1. The squares represent the Hopf bifurcation points. In the range "e" the laser shows excitable behaviour.

For $a_{SA} < 12\times10^{-12}$ m^{3}s^{-1} the laser shows either CW or nonlasing operation for any value of injected current. However, an increase of the differential gain coefficient of the SA causes the system to cross the Hopf bifurcation indicated by the solid thick line in Figure 9. Further increase of the differential gain coefficient of the SA results in a homoclinic bifurcation, which is denoted by the filled circle in Figure 6. Between the dotted and dashed lines, excitability is found to occur. The implication of the figure is that, to achieve excitability in practice by this approach, we need a sufficiently high value of SA differential gain coefficient. However, increasing the SA differential gain coefficient increases both the absorption level and the injected current.

As was mentioned above, the existence of excitability is determined by the carrier lifetimes, the absorption level in the saturable absorber and the cavity length. Let us now consider the case of a more pronounced excitability. Figure 10(a) shows the different types of system behaviour found in the photon number – injected current plane for large values of carrier lifetime in both the active and the SA regions (2ns) and high absorption level ($a = 23\times10^{-11}$m^{3}s^{-1}) with a 650 μm cavity length. When the injected current is smaller than 114 mA, the laser shows only CW operation, corresponding to the existence of a stable stationary state (stable focus). For injected currents between 114 and 124 mA, a linear stability analysis shows the existence of a saddle close to a stable node, which is well known to provide a mechanism for excitability. A confirmation that excitability is actually predicted in this case is given below. When the injected current is in the range 124-128 mA the laser shows SP operation, corresponding to the presence of a limit cycle. A further increase of injected current results in CW operation. As a result we are led to conclude that a large carrier lifetime in the SA, a high absorption level and a large cavity length are required to achieve pronounced excitability. Figure 10(b) shows the response of the laser to a sequence of injected current pulses with different amplitudes and delay times when it is in a state within the excitability region (circle in Figure 10(a)). There is a substantial response when an input pulse exceeds a certain threshold (such as for the first perturbation pulse) while the response to pulses below the threshold (such as

the third pulse) is much smaller. Comparison of the effect of the first and fourth pulses shows that the response is essentially independent of the perturbation amplitude as long as it is above threshold.

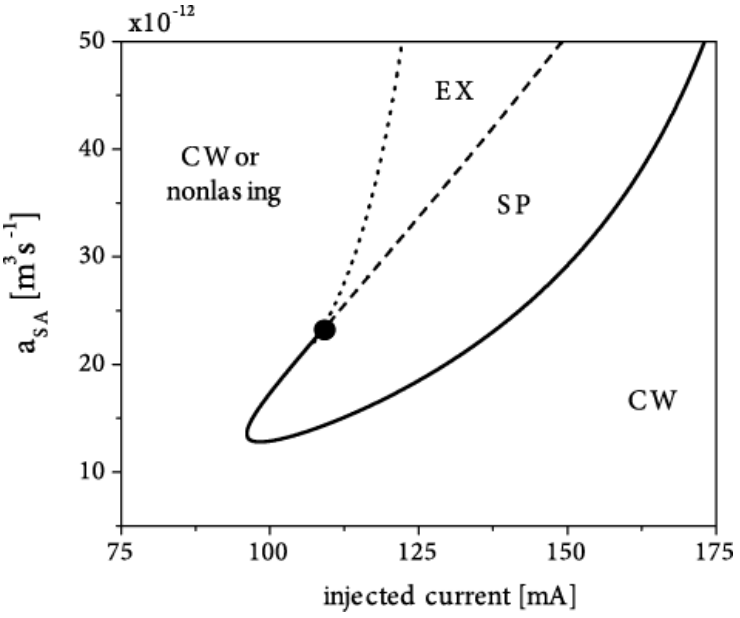

Figure 9. The bifurcation diagram in the plane of saturable absorber differential gain coefficient vs. injected current for a laser with a cavity length of 650 μm and a saturable absorber thickness of 2 nm. The carrier lifetimes in the active region and in the saturable absorber are 2 ns and 0.5 ns respectively. The other parameters are as in Table 1. The laser behaviour in the excitable region is denoted by EX. The solid line represents a Hopf bifurcation line.

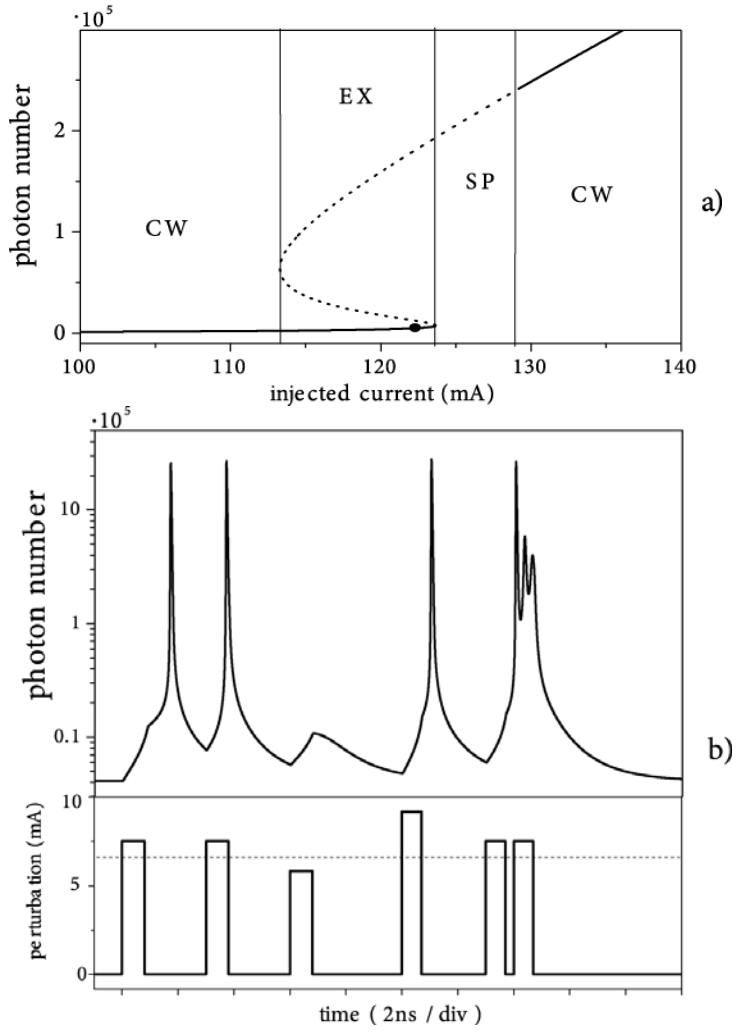

Figure 10. a) The different regimes of behaviour in the output number-injected current plane for a laser with a cavity length of 650 μm and saturable absorber thickness of 2 nm. The saturable absorber differential gain coefficient is fixed at 23×10^{-12} m^3s^{-1}, the carrier lifetimes are 2 ns in both active and saturable absorber regions. b) Response of the system to a train of pulses with different amplitudes and time separations perturbing the injected current. The initial conditions correspond to the circle in Fig. 10(a). The dotted line denotes the excitability threshold.

Further, there is evidence of a refractory period, since when the two pulses are separated by a sufficiently short time interval (such as the fifth and sixth pulses), the later pulse has an insignificant effect on the system. On the other hand there is a clear evidence of a significant response to both pulses when they are separated by a sufficiently large time interval (compare first and second pulses). Taken together the above properties are a clear indication of the presence of excitability in the system. Specifically, we have been able to confirm the three characteristics of excitability: the existence of a threshold above, which an excitation can occur; a response independent of the magnitude of a perturbation above the threshold; and the existence of a refractory period.

In conclusion it is important to emphasise that getting experimental excitable behaviour of InGaN lasers is still accompanied by significant difficulties. However, we expect that the phenomena of excitability could be observed in lasers with cavity lengths larger than 650 μm and a thick AlGaN layer, which results in a larger carrier life time in the SA. We believe that our work provides a good basis for future study and, in particular, provides some pointers for more detailed investigations of excitability and coherence resonance in InGaN lasers and their possible practical applications.

3. Tandem blue laser

3.1 Model and equations

Multi section lasers have been investigated for many years and, during the last few years, blue-violet tandem lasers of the type shown schematically in Figure 11 have been the subject of considerable attention. The devices used in our studies were fabricated structures grown by metal-organic chemical vapour deposition (for detail of the fabrication method, see [37]). The devices consist of two regions, *A* and *B*. Figure 11 shows a laser in which both regions are active as a result of the two injected currents I_1 and I_2 for the switch K in position 1. In contrast, for switch K in positions 2 and 3 the region A is active while region B acts as a SA layer.

The laser dynamics have been investigated using the single mode rate equations [32]

$$\frac{dS}{dt} = \left[\frac{L_A}{L} a_A \xi_A (n_A - n_{gA}) + \frac{L_B}{L} a_B \xi_B (n_B - n_{gB}) - G_{th} \right] S + M \left[a_A \frac{L_A}{L} \xi_A n_A + a_B \frac{L_B}{L} \xi_B n_B \right] \tag{5}$$

$$\frac{dn_A}{dt} = -\frac{a_A}{V_A} \frac{L_A}{L} \xi_A (n_A - n_{gA}) S - \frac{n_A}{\tau_A} + \frac{I_1}{eV_A} \tag{6}$$

$$\frac{dn_B}{dt} = -\frac{a_B}{V_B} \frac{L_B}{L} \xi_B (n_B - n_{gB}) S - \frac{n_B}{\tau_B} + \begin{cases} \dfrac{I_2}{eV_B} & K \ \ position \ 1 \\ -\dfrac{n_B}{T_d} & K \ \ position \ \ 2 \\ 0 & K \ \ position \ 3 \end{cases} \tag{7}$$

where *S* is the photon number, *L* is the cavity length of the full laser. The second term in the photon rate equation describes the spontaneous emission and *M* is the equivalent total number of the longitudinal modes, which is evaluated from the half-width of the linear gain spectrum. T_d is the effective diffusion lifetime. The subscripts *A* and *B* refer to regions A and B, respectively; $n_{A(B)}$ is the injected currier density, L_A and L_B are the cavity lengths, $a_{A(B)}$ are the dif-

ferential gain coefficients, $\xi_{A(B)}$ are the field confinement factors, which have been calculated for each design and taken to vary during the pulsations; $n_{gA(B)}$ are the transparency carrier densities, $\tau_{sA(B)}$ are the carrier lifetimes and $I_{1(2)}$ are the injected currents. The threshold gain level G_{th} is given by equation (4). The parameter values $\kappa = 20\,\mathrm{cm}^{-1}$, $a_A = 1.5\times10^{-12}\,\mathrm{m}^3\mathrm{s}^{-1}$, $a_B = 9.0\times10^{-12}\,\mathrm{m}^3\mathrm{s}^{-1}$, $\tau_{sB} = 1$ ns, ridge width 2 μm, active region thickness 16nm, and R_f=0.25, R_b=0.95 are used in the calculations that produced the results shown in figures 12-14**.**

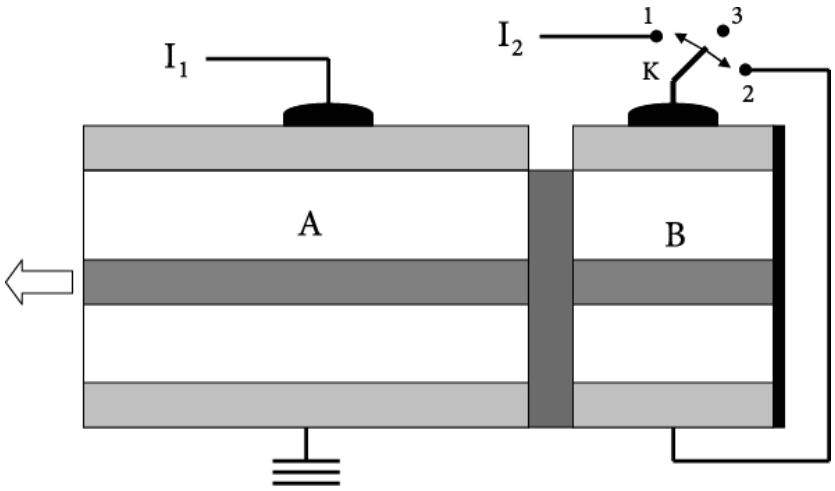

Figure 11. A schematic diagram of the blue tandem laser structure with two regions A and B. The contacts of region B have an electrical connection that can be broken by means of switch K. When K is in the position 1 current is injected into region A and region B and so that both can be active. The two cases when the switch K is in position 2 and in position 3 have been also investigated.

3.2 CW, SP and excitability of tandem lasers

The numerical calculations have been carried out by solving equations (5)-(7) for the three cases shown in Figure 11:

- model (1) when the two injected currents are supplied –switch K in position 1
- model (2) when the switch K is in position 2
- model (3) when the switch K is in position 3

When currents are injected into regions *A* and *B*, switch K in position 1, both regions can be active. The calculated dependence of the photon number *S* on the current injected into region *A* for different injected currents in region *B* is shown in Figure 12. For a current of 20mA injected into region B, the threshold current of region A is estimated to be 55 mA. A decrease of injected current in region B leads to an increase of the threshold current of region A up to a value of approximately 110 mA. When the injected current in region B is decreased below 10 mA, the s-shaped curves in Figure 12 suggest that there is a non-smooth dependence of output power on injected current which is also seen in the experimental results. In this regime it should be possible to switch between two states. We also note that only CW operation has been observed in the experiment.

In the case of model (1), the laser diode needs two current sources and, in any case, experimental evidence for SP has not yet been achieved. An alternative approach is the model (2) where a current is only injected into region A and the contacts of region B have an electrical connection that can be broken by means of switch K in position 3.

We now examine the behaviour of the device when the switch K is in position 2 or 3. Figure 13a shows the calculated dependence of the photon number *S* on the injected current in the region A when the switch K is in position 3 (thin line) and in position 2 (solid line). When the switch is in position 3 regions A and B are similar in nature; they are made of

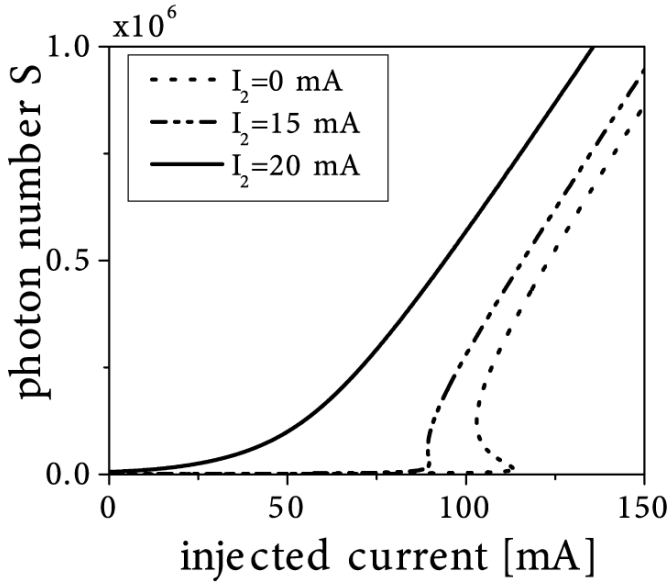

Figure 12. The dependence of photon number *S* on the current injected into region A for different values of the current injected into region B. The cavity lengths are 500μm and 200 μm for regions A and B, respectively. The other parameters used in the calculations are: n_{gA}=1.8×10^{25} m^{-3}, n_{gB}=1.0×10^{25} m^{-3}, τ_{sB}=1.0 ns.

the same materials and differ only in that one is active as a result of current injection. As a result, the carrier lifetime in both can be assumed to have the same value ($\tau_{sA} = \tau_{sB} = 1.0\ ns$). Only CW operation described by the thin line in Figure 13a is predicted in this case. However, when the switch is in position 2, the carrier lifetime in region B can be expected to become much smaller as a result of carrier diffusion.

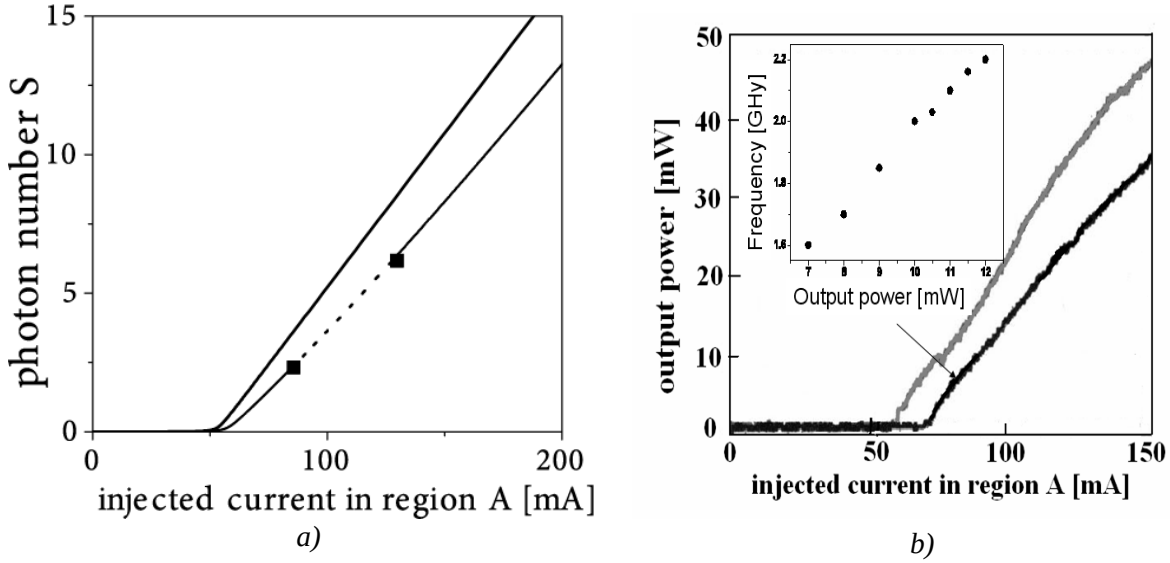

Figure 13. The dependence of the photon number *S* on the current injected into region A for the case when the switch K is in position 2 and in position 3. Left: Numerical calculations: Thin line – the switch K is in position 3 and $\tau_{sA} = \tau_{sB} = 1.0$ ns, $n_{gA} = 2.3\times10^{25}$ m^{-3}, $n_{gA} = 1.3\times10^{25}$ m^{-3}. Thick line – the switch K is in position 2 and $\tau_{sA} = 1.0$ ns, $\tau_{SB} = 0.1$ ns, $T_B = 0.1$ ns, $n_{gA} = 2.3\times10^{25}$ m^{-3}, $n_{gB} = 0.1\times10^{25}$ m^{-3}, $a_A = 1.5\times10^{-12}$ m^{3}s^{-1}, $a_B = 9.0\times10^{-12}$ m^{3}s^{-1}. The dotted line terminated by squares represents the SP region. The cavity lengths of regions A and B are 490μm and 52.3μm respectively. Right: the experimentally observed dependence of output power on the current injected into region, respectively [37,32]. The inset shows the dependence of SP frequency on output power when SP occurs.

The relation between the gain coefficient and the electron density is nonlinear, but is approximated with two lines around the operating point. Then different values for the carrier density for transparency are introduced in the analysis. Region B acts as a SA and a small carrier lifetime can provide the conditions for SP to occur. If the lifetime in the SA is taken as 0.1 ns, SP is predicted to occur in the range of current values from 85 mA to 125 mA denoted by the dotted line terminated by squares in Figure 13a. The squares indicate Hopf-bifurcation points. Experimental confirmation [32, 37] of the predicted behaviour is shown in Figure 13b, where the grey line gives the dependence of output power on injected current in region A for the case when the switch K in position 3. Only CW operation was observed despite a careful search for SP. The black line in Figure 13b gives the corresponding experimental results when the switch K is in position 2. In this case SP was observed accompanied by a small increase of threshold current. Comparison of Figures 13a and 13b shows, that there is a good agreement between the results of the numerical calculations and the experimental data. The inset of Figure 13b shows the dependence of SP frequency on output power with SP in the range 1.6 GHz up to 2.2 GHz. The presence of hysteresis is evident in Figure 12. Thus, this is the first indication that the phenomenon of excitability might be possible.

Now, we will focus on the study of the laser behaviour in the case when the switch K is in position 3 (Figure 11). Figure 14 shows the bifurcation diagram in the parameter plane of region B cavity length versus injected current of region A. The solid line shows the Hopf-bifurcation points, which are terminated by the saddle–node bifurcation, marked by a circle. A linear stability analysis shows that in the region EX a node, a saddle and an unstable focus coexist and the system behaves as an excitable one. In the numerical calculations we have also confirmed the three characteristics of excitability: the existence of a threshold above, which an excitation can occur; a response independent of the magnitude of a perturbation above the threshold; and the existence of a refractory period.

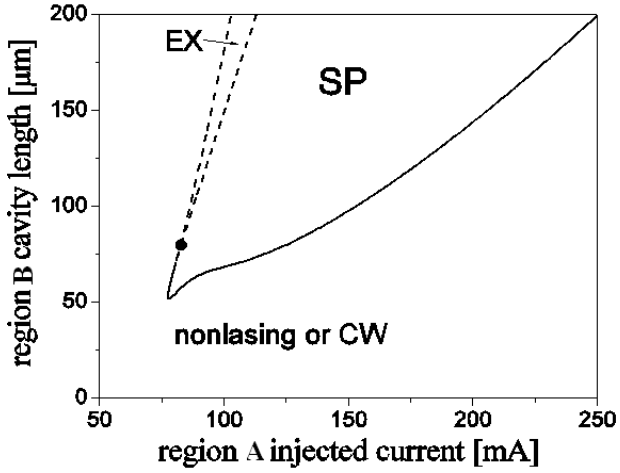

Figure 14. Bifurcation diagram in the $L_B - I_1$ plane; the switch K in Fig.11 is in position 3. The parameters are L_A=500μm, $n_{gA}=1.8\times10^{25}\text{m}^{-3}$, $n_{gB}=1.0\times10^{25}\text{m}^{-3}$, τ_{sB}=1.0ns. The circle denotes the point of saddle node bifurcation.

In summary, we expect that the phenomena of excitability could be observed in lasers with a cavity length larger than 650 μm and a thick AlGaN layer, which results in the larger carrier lifetime in the SA. We believe that our work provides a good basis for future study. In particular it provides some pointers for more detailed investigations of excitability and coherence resonance in InGaN lasers and their possible practical applications.

4. Conclusions

In this review we have investigated the CW, self-pulsating (SP) and excitable behaviour of blue InGaN lasers with different saturable absorber (SA) designs. The roles of the SA prop-

erties have been pointed out with a view to controlling laser output characteristics. Two laser structures have been investigated: one with a SA grown parallel to the active medium and a tandem laser. For lasers with a SA grown parallel to the active layer, a bifurcation analysis shows that a Hopf bifurcation is responsible for the appearance of SP under suitable conditions. Also two different possibilities to obtain excitable behaviour of the devices have been discussed. It has been shown that a relatively short carrier lifetime in the SA is required for SP, whereas a large one is more appropriate for excitable behaviour. Large cavity length and high SA differential gain coefficient are also favourable for pronounced excitability. For the tandem laser it was found that an injected current in region B implies a low threshold current in region A but it results only in CW operation. We have also demonstrated the SP operation of a tandem InGaN laser with an externally controlled circuit. The conditions for SP have been predicted by calculations based on a single mode rate equation model of the device. SP has also been achieved in experiments on fabricated lasers with properties very similar to those predicted theoretically. Finally, we believe the results presented suggest that the proposed new design of a blue laser is promising for the production of self-pulsating lasers with improved performance.

Acknowledgements

This work has been carried out with the financial support of the Alexander von Humboldt Foundation, Germany, The Royal Society, UK, the JSPS, Japan, and the 307 b/s project, Moldova. The author would like to thank R.A. Abram for reading the manuscript and Minoru Yamada for detailed discussions. Many thanks are also due to T. Kawakami, T. Ohno, S. Ito, and M. Taneya from the Devices Technology Research Laboratories, Sharp Corporation, Japan for their experimental support.

References

[1] http://www.blu-ray.com/

[2] S. Nakamura, S. Pearton, and G. Fasol, The Blue LaserDiode, 2nd ed. Berlin, Germany: Springer, 2000.

[3] S. Nakamura, M. Senoh, S. Nagahama, N. Iwasa, T. Yamada, T. Matsushita, Y. Sugimoto, and H. Kiyoku, “Optical gain and carrier lifetime of InGaN multi-quantum well structure laser diodes”, Appl. Phys.Lett., 69, 1568–1570, (1996).

[4] T. Takeuchi, H. Takeuchi, S. Sota, H. Sakai, H. Amano, and I. Akasaki, “Optical properties of strained AlGaN and GaInN on GaN”, Jpn. J. Appl. Phys., 36, L177–179, (1997).

[5] T. Kobaiasi, T. Kobayashi, F. Nakamura, K. Naganuma, T. Tojyo, H. Nakajima, T. Asatsuma, H. Kawai, and M. Ikeda, “Room-temperature continuous-wave operation of GaInN/GaN multiquantum well laser diode”, Electron. Lett., 34, 1494–1495, (1998).

[6] A. Kuramata, S. Kubota, R. Soejima, K. Domen, K. Horino, and T. Tanahashi, “Room-temperature continuous wave operation of InGaN laser diodes with vertical conducting structure on SiC substrate”, Jpn. J. Appl. Phys., 37, L1373–L1375, (1998).

[7] M. Kuramoto, C. Sasaoka, Y. Hisanaga, Y. Hisanaga, A. Kimura, A.A. Yamaguchi, H. Sunakawa, N. Kuroda, M. Nido, A. Usui, and M. Mizuta, “Room-temperature continuous-wave operation of InGaN multi-quantum -well laser diodes groun on an n-GaN substrate with a backside n contact”, Jpn. J. Appl. Phys., 38, L184–L186, (1999).

[8] M. Kneissl, D.P. Bour, C.G. Van de Walle, L.T. Romano, J.E. Northrup, R.M. Wood, M. Teepe, and N.M. Johnson, “Room-temperature continuous wave operation of InGaN

multiple-quantum-well laser diodes with an asymmetric waveguide structure", Appl. Phys. Lett., 75, 581, (1999).
[9] http://www.nichia.co.jp
[10] S. Nakamura, M. Senon, S. Nagahama, N. Iwasa, T. Yamada, T. Matsushita, H. Kryoku, Y. Sugimoto, T. Kozaki, H. Umemoto, M. Sano, and K. Chocho, "InGaN/GaN/AlGaN – based laser diodes with modulation -doped strained-layer superlattices", Jpn. J. Appl. Phys., vol. 36, L1568, (1997).
[11] M. Yamada, "Theoretical analysis of noise-reduction effect in semiconductor laser with help of self-sustained pulsation phenomena", J. Appl. Phys., 79, 61–71, (1996).
[12] S. Matsui, H. Takiguchi, H. Hayashi, S. Yamamoto, S. Yano, and T. Hijikata, "Suppression of feedback-induced noise in short-cavity V-channeled substrate inner stripe lasers with self-oscillation", Appl. Phys. Lett., 43, 219–221, (1983).
[13] S. Yamashita, A. Ohishi, T. Kajimura, M. Inoune, and Y. Fukui, "Low-noise AlGaAs lasers grown by organo-metallic vapor phase epitaxy", IEEE J. Quantum Electron., 25, 1483–1388, (1989).
[14] H.-J. Wünsche, M. Radziunas, S. Bauer, O. Brox, B. Sartorius, Modeling of mode control and noise in self-pulsating PhaseCOMB lasers, IEEE Journal on Selected Topics in Quantum Electronics, 9, no. 3, 857- 864, (2003).
[15] Martin Möhrle, Bernd Sartorius, Carsten Bornholdt, Stefan Bauer, Olaf Brox, Ariane Sigmund, Ralf Steingrüber, Mindaugas Radziunas, and Hans-Jürgen Wünsche, Detuned grating multi-section-RW-DFB-lasers for high speed optical signal processing, IEEE Selected Topics on Quantum Electronics, 7, no. 2, 217-223, (2001).
[16] U. Bandelow, H.-J. Wünsche, and B. Sartorius, Dispersive self Q-switching in DFB-lasers: theory versus experiment IEEE Journal of Selected Topics in Quantum Electronics, 3, 270-278, (1997).
[17] C.O. Weiss and R.Vilaseca, Dynamics of Lasers. Germany: VCH Weinheim, 1991.
[18] Y.I. Khanin, Principles of Laser Dynamics. Amsterdam, The Nether-lands: Elsevier, 1995.
[19] U. Bandelow, H.-J. Wünsche, and B. Sartorius, Dispersive self Q-switching in DFB-lasers: theory versus experiment, IEEE Journal of Selected Topics in Quantum Electronics, 3, 270-278, (1997).
[20] B. Sartorius, M. Möhrle, S. Reichenbacher, H. Preier, U. Bandelow, and H.J. Wünsche, Dispersive self Q-switching in self-pulsating DFB lasers, IEEE J. of Quantum Electronics, 33, 211-218, (1997).
[21] M. Radziunas, H.-J. Wünsche, B. Sartorius, O. Brox, D. Hoffmann, K. Schneider, D. Marcenac, Modelling Self-Pulsating DFB Lasers with Integrated Phase Tuning Section, IEEE Journal of Quantum Electronics, 36, 1026-1034, (2000).
[22] J.D. Murray, Mathematical Biology, Springer, 1990.
[23] S. Grill, V.S. Zykov, and S.C. Mueller, J. Phys. Chem. 100, 19082, (1996).
[24] W. Lu, D. Yu, and R.G. Harrison, Phys. Rev. A 58(2), R809, (1998).
[25] V.Z. Tronciu and R.A. Abram "Excitability of excitons and biexcitons in a ring cavity", Phys. Rev. E., 65, 026616, (2002).
[26] J.L.A. Dubbeldam, B. Krauskopf, and D. Lenstra, Phys. Rev. E 60(6), 6580, (1999).
[27] M. Giudici, C. Green, G. Giacomelli, U. Nespolo, J.R. Tredicce, Phys. Rev. E 55, 6414, (1997); M. Giudici, C. Green, G. Giacomelli, U. Nespolo, J.R. Tredicce, Phys. Rev. E 58, 4043, (1998); G.H.M. Van Tartwijk, I. Fischer, Phys. Rev. E 58, 4041, (1998); E.A. Viktorov, P. Mandel, Phys. Rev. Lett., 85, 3157, (2000); J.R. Tredicce, AIP Conference Proceedings, 548, 238, (2000).

[28] V.Z. Tronciu, H.J. Wünsche, K. Schneider and M. Radziunas, "Excitability of lasers with integrated dispersive reflector", SPIE Proceedings, 4283, 347-354, (2001).
[29] H.J. Wünsche, O. Brox, M. Radziunas and F. Henneberger, "Excitability of a Semiconductor Laser by a Two-Mode Homoclinic Bifurcation", Phys. Rev. Lett., 88, 023901, (2002).
[30] M.A. Larotonda, A. Hnilo, J.M. Mendez, A.M. Yacomotti, Phys. Rev. A, 65, 033812, (2002).
[31] V.Z. Tronciu, M. Yamada, Tomoki Ohno, Shigetoshi Ito, Toshiyuki Kawakami, and Mototaka Taneya. "Self-pulsation in an InGaN laser - theory and experiment", IEEE J. Quantum Electronics, 39, no. 12, 1509-1514, (2003).
[32] V.Z. Tronciu, M. Yamada Toshiyuki Kawakami, Shigetoshi Ito, Tomoki Ohno Mototaka Taneya and R.A. Abram "The theoretical and experimental investigation of the dynamics of tandem blue-violet lasers", Optics Communications, 235/4-6, 409-414, (2004).
[33] V.Z. Tronciu, M. Yamada, Tomoki Ohno, Shigetoshi Ito, Toshiyuki Kawakami, and Mototaka Taneya, Analysis of self-pulsation characteristics of InGaN laser diode, Phys.Stat.Sol. C, 7, 2296-2299, (2003).
[34] V.Z. Tronciu**,** M. Yamada and R.A. Abram, Toshiyuki Kawakami, Tomoki Ohno, Shigetoshi Ito, and Mototaka Taneya, Self-pulsation and excitability InGaN lasers, Weierstrass Institute for Applied Analysis and Stochastic Preprint, No. 940, 11 pages, (2004).
[35] V.Z. Tronciu, M. Yamada and R.A. Abram, Investigation of self-pulsation and excitability of tandem blue lasers. The AIUB Journal of Science and Engineering, 3, No.1, 7, (2004).
[36] V.Z. Tronciu, Minoru Yamada, and R.A. Abram, Analysis of the dynamics of a blue-violet InGaN laser with saturable absorber. Phys. Rev. E 70, 026604, (2004).
[37] T. Ohno, S. Ito, T. Kawakami and M. Taneya, "Self- pulsation in InGaN laser diodes with saturable absorber layers", Appl. Phys. Lett., 83, 1098-1102, (2003).
[38] M. Yamada, "A theoretical Analysis of self- sustained pulsation phenomena in narrow-stripe semiconductor lasers", IEEE J. Quantum Electron., 29, 1330-1336, (1993).
[39] M. Yamada, "A theoretical analysis of quantum noise in semiconductor laseroperating with self-sustained pulsations", IEICE Trans. Electron., E81-C, 290–298, (1998).
[40] M. Yamada, "Variation of intensity noise and frequency noise with spontaneous emission factor in semiconductor laser", IEEE J. Quantum Electron., 30, 1511–1519, (1994).
[41] T.L. Paoli, "Saturable absorption effects in the self-pulsing (AlGa)As junction laser", Appl. Phys. Lett., 34, 652–655, (1979).
[42] M. Ueno and R. Lang, "Conditions for self-sustained pulsation and bistability in semiconductor lasers", J. Appl. Phys., 58, 1689–1692, 1985.
[43] M.J. Adams and C. Sinthanayothin, "Large-signal analysis of self-pulsating laser diodes", Proc. SPIE, 2994, 513–519, (1998).
[44] E.A. Avrutin, "Analysis of spontaneous emission and noise in self-pulsing laser diodes", Proc. Inst. Elect. Eng., pt. J, 140, 16–20, (1993).
[45] U. Bandelow, H.-J. Wünsche, and H. Wenzel, "Theory of self-pulsations in two-section DFB lasers", IEEE Photon. Technol. Lett., 5, 1176–1179, (1993).
[46] H. Wenzel, U. Bandelow, H.-J. Wünsche, and J. Rehberg, "Mechanisms of fast self-pulsations in two-section DFB lasers", IEEE J. Quantum Electron., 32, 69–78, (1996).
[47] U. Bandelow, H.-J, Wünsche, B. Sartorius, and M. Mohrle, "Dispersive self-Q-switching in DFB lasers-theory versus experiment", IEEE J.Select. Topics Quantum Electron., 3, 270–278, (1997).

[48] J.L.A. Dubbeldam and B. Krauskopf, “Self-pulsations of lasers with saturable absorber: Dynamics and bifurcations”, Opt. Commun., 159, 325–338, (1999).
[49] C.R. Mirasso, G.H.M. van Tartwijk, E. Hernandez-Garcia, D. Lenstra, S. Lynch, P. Landais, P. Phelan, J.O’Gorman, M.S. Miguel, and W. Elsaer, “Self-pulsating semiconductor lasers: Theory and experiment”, IEEE J. Quantum Electron., 35, 764–770, (1999).
[50] Y.D. Jho, J.S. Yahng, E. Oh, and D.S. Kim, “Measurement of piezoelectric field and tunneling times in strongly biased InGaN/GaN quantum wells”, Appl. Phys. Lett., 79, 1130-1132, (2001).
[51] C.-K. Sun and T.-L. Chiu, “Time resolved photoluminescence studies of InGaN/GaN single-quantum-wells at room temperature”, Appl. Phys. Lett., 71, 425–427, (1997).